

**Revision of global carbon fluxes based on a reassessment of oceanic
and riverine carbon transport**

Authors: L. Resplandy^{1*}, R. F. Keeling², C. Rödenbeck³, B. B. Stephens⁴, S. Khatiwala⁵, K. B. Rodgers⁶, M. C. Long⁴, L. Bopp⁷ and P. P. Tans⁸

Affiliations:

¹Princeton University, Department of Geosciences and Princeton Environmental Institute.

²Scripps Institution of Oceanography, UCSD, La Jolla, USA.

³Max Planck Institute for Biogeochemistry, Jena, Germany.

⁴National Center for Atmospheric Research, Boulder, USA.

⁵Department of Earth Sciences, University of Oxford, Oxford OX1 3AN, UK.

⁶Program in Atmospheric and Oceanic Sciences, Princeton University, Princeton, USA.

⁷Laboratoire de Météorologie Dynamique / Institut Pierre Simon Laplace, CNRS / ENS / Ecole Polytechnique / Sorbonne Université, Département de Géosciences, Ecole Normale Supérieure, Paris.

⁸Earth System Research Laboratory, NOAA, Boulder, USA.

*Correspondence to: laurer@princeton.edu

Measurements of atmospheric CO₂ concentration provide tight constraints on the sum of the land and ocean sinks. This constraint has been combined with estimates of the ocean carbon flux and the riverine transport of carbon from land to oceans to isolate the land

sink. Uncertainties in the ocean and river fluxes therefore translate into uncertainties in the land sink. Here, we introduce a heat-based constraint on the latitudinal distribution of ocean and river carbon fluxes, and reassess the partition between ocean, river and land in the tropics, and in the southern and northern extra-tropics. We show that the ocean overturning circulation and biological pump tightly link the ocean transports of heat and carbon between hemispheres. Using this coupling between heat and carbon, we derive ocean and river carbon fluxes compatible with observational constraints on heat transport. This heat-based constraint requires a 20% to 100% stronger ocean and river carbon transport from the Northern Hemisphere to the Southern Hemisphere than existing estimates, and supports an upward revision of the global riverine carbon flux from 0.45 to 0.78 PgC/y. These systematic biases in existing ocean/river carbon fluxes redistribute up to 40% of the carbon sink between northern, tropical and southern land ecosystems. As a consequence, the magnitude of both the southern land source and the northern land sink may have to be substantially reduced.

Studies over the past 25 years support the existence of a large net land biospheric CO₂ sink (e.g. 0.5 to 2 PgC/yr)¹⁻³, dominated by a growing uptake in the Northern Hemisphere⁴⁻⁹. A primary basis for quantifying the land sink is from atmospheric CO₂ measurements using atmospheric inverse calculations². These atmospheric inversions give fairly consistent short-term variations (seasonal to interannual) of the land sink over the past two decades^{2,10}. Yet, significant uncertainties remain on the long-term partitioning between northern, tropical and southern land sinks^{6,11}. The potential for systematic error in inverse calculations weakens our ability to predict

the response to anthropogenic changes and evaluate allowable carbon emissions compatible with mitigation strategies.

Uncertainties over the land sink magnitude and latitudinal distribution are in part connected to the uncertain impact of natural carbon fluxes on atmospheric CO₂. In inverse calculations, the sink emerges from the difference between observed CO₂ concentrations and the pattern expected from other processes including fossil fuel emissions¹², seasonal exchanges with the terrestrial biosphere¹³, ocean anthropogenic carbon uptake¹⁴, and natural flows of carbon linked to ocean circulation and rivers^{15,16}. These natural flows include a north-south loop that uptakes atmospheric carbon on land and over the ocean in the Northern Hemisphere, transports carbon from land to ocean, and releases carbon in the Southern Ocean^{17,18}. This ocean/river loop, which carries carbon southward and is balanced by a return flow through the atmosphere, existed pre-industrially and is still influencing atmospheric CO₂ gradients today. Recent work has improved the quantification of fossil fuel emissions^{12,19,20} and seasonal effects¹¹. As a result, the sum of the ocean, river, and land fluxes is better constrained. Yet the land sink itself is still very sensitive to uncertainties in the ocean/river flux latitudinal distribution used as a-priori constraints by atmospheric inversions²¹. Two major issues with state-of-the-art atmospheric inversions are the excessive CO₂ emissions from the land in the Southern extra-tropics (7 of 11 models in²) and a considerable Northern extra-tropical land sink compared to terrestrial ecosystem models and inventories^{6,22,23} (9 of 11 models with 2000-2004 sink > 1.3 PC/y²). Here we show that previous estimates of the ocean/river loop were biased low, and that correcting this bias leads to a reduction in both the southern land source and northern land sink in atmospheric inversions.

To expose this bias, we introduce a heat-based constraint on the latitudinal distribution of natural ocean/river carbon fluxes. The heat constraint is relevant because the north-south carbon loop is largely driven by the overturning circulation, which also transports heat, leading to a coupling between carbon and heat transports.

Tight coupling between heat and carbon transports

We first demonstrate that there is a strong heat-carbon coupling at the scale of individual ocean basins by examining the meridional ocean transports of heat and natural carbon in hydrographic data and in 11 models (9 Earth system and 2 ocean models, Fig 1A). In the Atlantic Ocean, observations and models fall along a consistent linear relationship corresponding to a southward transport of 0.3 PgC/y per PW of northward heat transport. In the Indo-Pacific, where only model results are available, simulated transports line along this same relationship, but with larger residuals in the south. This link between carbon and heat partly arises from the control of temperature-driven solubility changes in regulating annual CO₂ annual exchanges with the atmosphere (CO₂ more soluble in colder waters)^{24,25}. The carbon-to-heat ratio of -0.3 PgC/y per PW is however a third of the value expected from solubility alone (-0.9 PgC/y per PW). This lower ratio is related to the biological carbon pump, i.e. the export and decomposition of organic matter that maintain high dissolved inorganic carbon concentrations at depth. The thermal carbon uptake at high-latitude is dampened because of the excess carbon brought to the surface in these regions by bi-directional vertical exchange with the deep ocean (Fig 1B). Nevertheless, this biological dampening effect largely correlates with temperature, which explains the overall robust carbon-to-heat ratio of -0.3 PgC/y per PW. As a result, the Atlantic Meridional

Overturning Circulation transports warm surface waters northward and cold carbon-rich deep waters southward, and the gyre circulation in the Indo-Pacific Ocean transports warm surface waters poleward and carbon-rich deep waters equatorward (Fig 1).

Despite the correlation between biological and thermal effects, the biological effect is also influenced by the degree to which upwelled carbon is re-exported to depth as sinking organic particles. This process introduces some decoupling between heat and carbon, mostly in the deep overturning cell involving Antarctic Bottom Water, which exchanges with the atmosphere principally in the Southern Hemisphere (Fig 1 B). This deep cell contributes little to the heat transport, as heat is nearly conserved along the loop, but contributes to the southward carbon transport, as carbon from the decomposition of sinking detritus accumulates along the loop before being outgassed in the south (Fig 1 C). This decoupling is stronger in the older waters of the South Indo-Pacific, yielding larger model residuals in this region due to inter-model differences in biological pump and deep cell transport (Fig 1 A).

A strong coupling between heat and carbon is also found at global interhemispheric scale. Across the 11 models, we find that the following relationship explain 85% of the variance in interhemispheric carbon transport:

$$A_C = -0.31 (\pm 0.15) \times A_Q + 0.19 (\pm 0.10) \times A_{\text{BioPump}} - 0.65 \quad (r^2 = 0.85) \quad (\text{Eq 1})$$

Here A_C (Pg yr^{-1}) and A_Q (PW) are the interhemispheric “transport asymmetries” of carbon and heat, defined as the average of the global transports across 20°N and 20°S , and A_{BioPump} (Pg yr^{-1}) the “biological pump asymmetry”, defined as the imbalance between the particulate carbon flux exported below 100 m south of 20°S and north of 20°N (Figure 2). The relationship between Eq

(1) and individual model results is shown in Figures 3 and S1. A_C and A_Q would be zero if the transports across 20°N and 20°S were opposed and of same magnitude. A_{BioPump} would be zero if the particulate flux poleward of 20° were equal. In reality, the ocean takes up more natural carbon, loses more heat and export less particles in the North. A_C is therefore oriented southward (negative), A_Q and A_{BioPump} are northward (positive). Note that estimates of A_C in Eq. (1) involve small corrections for the river loop, since river influences were neglected in some models (see methods). We find that carbon and heat transports are linked at the hemispheric scale with 0.31 ± 0.15 PgC/y transported southward per PW of heat transported northward, which is fully consistent with the relationship found in individual ocean basins in observations and models (Fig 1A). In Eq. (1) A_{BioPump} is diagnostic of the residual biological influences (deep cell decoupling) not already incorporated into the A_Q term. A link between this residual effect and the high-latitude particulate flux is expected, because of the role the downward particle flux plays in countering the upwelling of carbon rich water from depth. This linkage makes A_{BioPump} a useful measure of the model differences in heat/carbon decoupling, that we can exploit to constrain A_C .

Heat constraint on ocean/river carbon fluxes

An accurate determination of A_C is critical to establishing the north-south distribution of land carbon sinks using atmospheric inversions. To refine A_C , we use Eq. (1) and estimates of A_{BioPump} and A_Q . Globally, two independent lines of evidence, based on atmospheric and satellite observations²⁶ and on atmospheric O_2 and CO_2 distributions²⁷, give a reasonably strong constraint on the heat asymmetry $A_Q = 0.9 \pm 0.2$ PW, also in the range of looser constraints from hydrographic sections²⁸. In contrast, the biological carbon pump and hence A_{BioPump} are very

poorly constrained by observations^{29–32}. We therefore use $A_{\text{BioPump}} = 2.2 \pm 1$ PgC/y, based on the model ensemble mean value and its large uncertainty range ($\pm 2\text{-}\sigma$ range, Fig S1).

Applying $A_Q = 0.9 \pm 0.2$ PW and $A_{\text{BioPump}} = 2.2 \pm 1$ PgC/y in Eq. (1) yields $A_C = -0.52 \pm 0.23$ PgC/y, not far outside of the model range making it relatively robust (Fig. 3). Compared to observations ($A_Q = 0.9 \pm 0.2$ PW), the 11 models considered here fall short in their estimate of A_Q , and the strong A_C to A_Q relationship therefore implies that carbon asymmetries A_C in these models are also biased low. The deficiencies of ocean forward models in their heat transport have been discussed previously, and arise mostly from shallower and warmer deep southward flow in the Atlantic Ocean^{27,33,34} and from deficiencies in western boundary currents³⁵. However, the systematic bias these deficiencies introduce in carbon fluxes have been largely overlooked³⁶. Furthermore, we find that our estimate is more than twice the transport $A_C = -0.19 \pm 0.09$ PgC/y obtained from ocean inverse calculations used to derive ocean/river fluxes^{21,27,37–40} (Fig. 4 case A). This is to be expected as ocean inverse models use observed tracer distributions in combination with the transport from forward models and therefore share their bias in A_C and A_Q (Fig S4). We also find that models optimized using hydrographic data^{27,40} only marginally improve heat and carbon asymmetries (Fig S4 and SI). Earlier applications of ocean inverse and forward calculations assumed that the ocean interhemispheric carbon transport lied in the range of available inverse models^{37,41–43} but our result show this assumption is probably incorrect.

While our estimate of A_C is incompatible with ocean inversion-based fluxes, it is not incompatible with fluxes based on observed surface partial pressure of CO_2 ($p\text{CO}_2$)^{44–47}. $p\text{CO}_2$ -based estimates of modern air-sea CO_2 fluxes⁴⁴ yield a transport asymmetry $A_C = -0.35 \pm 0.21$

PgC/y, once the ocean anthropogenic carbon sink is removed^{14,48} and the river carbon discharge of Jacobson et al.³⁸ is accounted for (see methods). This result is not strongly dependent on the choice of the pCO₂-based fluxes, as shown in several alternate versions, and lies in the lower range of our heat-based constraint $A_C = -0.52 \pm 0.23$ PgC/y (Fig. 4 cases B-D).

Impact on land anthropogenic sink

To evaluate the impact of the carbon asymmetry on land sink estimates, we use the Jena CarboScope atmospheric CO₂ inversion⁴⁹ (atmosphere transport model TM3) and two sets of ocean/river carbon fluxes. The first set uses the ocean inversion-based steady-state fluxes⁴¹ characterized by a weak carbon transport asymmetry $A_C = -0.19 \pm 0.09$ PgC/y (Fig 4 case A) combined with anthropogenic fluxes¹⁴. For the second set, we combine a pCO₂-based air-sea CO₂ flux⁴⁴ and a river discharge which scales up the river fluxes of Jacobson et al.³⁸ by a factor 1.73. This upscaling increases the global discharge from 0.45 ± 0.23 to 0.78 ± 0.41 PgC/yr, and intensifies the river contribution to A_C from -0.15 to -0.26 PgC/y, yielding $A_C = -0.43$ PgC/y (Fig 4 case E). The exact value of 1.73 is not critical here, but was chosen, as described below, because it simultaneously optimizes the global ocean carbon budget and yields A_C near the center of the heat-based constraint.

The impact of the two ocean/river fluxes on land fluxes for the 1990-2010 period is shown in Figure 5. Using the ocean inversion-based flux yields a strong northern land sink (2.56 PgC/y) and strong sources from the southern (0.34 PgC/y) and tropical (0.95 PgC/y) land. In contrast, the pCO₂-based flux yields a weaker land source in the Southern Hemisphere (0.10 PgC/y vs. 0.34 PgC/y), a weaker land sink in the Northern Hemisphere (2.26 PgC/y vs. 2.56 PgC/y) and a

slightly weaker tropical land source (0.89 vs. 0.95 PgC/y). Overall, this shows a redistribution of ~40% of the land carbon sink (~0.5 PgC/y for 1990-2010).

Multiple lines of evidence support revised carbon budget

The revised ocean/river flux proposed here is more concordant with oceanic and atmospheric constraints than previous estimate central values, as shown by five independent lines of evidence. First, the revision is consistent with the heat-based empirical constraint and with pCO₂ data. Second, it is in optimal accord with best estimates of the global ocean carbon sink (air-sea + river = global ocean sink). Without the river upscaling, the central estimate of the pCO₂-based air-sea flux (1.4 PgC/y in 2000⁴⁴) and of the river flux (0.45 PgC/y³⁸) fall short in matching the estimates of the net global ocean sink (2.18 PgC/y^{14,48}, Tab. S5).

Third, the revision establishes a more credible distribution of land sinks by reducing the strong southern land source, which is a questionable feature of many recent atmospheric inversions². This source needed to compensate an excessively strong ocean carbon sink in the southern extra-tropics is implausible because of the absence of major land ecosystems south of 20°S. Our result suggests that the Southern Ocean carbon sink is weaker than previously thought (Fig 5). Our revision also reduces the northern land sink, in line with studies suggesting that atmospheric inversions overestimate this sink compared to bottom-up ecosystem models and inventories^{11,22,23}. It also yields a small reduction of the tropical land source, which reinforces the idea that atmospheric inversions overestimate the tropical land source and that a larger carbon sink is needed in tropical intact ecosystems to offset land use emissions^{3,6,11,50}. Remaining uncertainties

in the model used here (TM3) and other atmospheric transport models leave room to further increase the intact tropical ecosystems uptake and reduce the gap with bottom-up estimates.

Fourth, the revised fluxes provide a relatively simple explanation for the evolution of the inter-hemispheric atmospheric CO₂ gradient, which increased quasi-linearly with fossil-fuel burning, but with a non-zero intercept of -0.55 ± 0.15 ppm (Fig 6). A simple dependence of this gradient on fossil-fuel burning can be explained by burning mostly occurring in the Northern Hemisphere, and assuming land sinks have evolved gradually with a history similar to that of fossil-fuel burning⁵. As shown in SI, the steady-state ocean/river transport required by the heat constraint ($A_C = -0.52 \pm 0.23$ PgC/y) is able to maintain a stationary atmospheric CO₂ gradient between -0.7 and -0.4 ppm, consistent with the intercept (-0.55 ± 0.15 ppm, Fig. 6 and S5). This perspective, also consistent with atmospheric ¹³C gradients analyses⁵, suggests that the natural ocean/river loop could sustain a pre-industrial inter-hemispheric atmospheric CO₂ gradient without necessarily invoking large shifts in land sinks prior to 1958^{51,52}.

Fifth, the revised fluxes are in reasonable accord with current understanding of river contributions to within their wide uncertainties. Despite early interpretations^{16,17,38}, the river fluxes have been largely overlooked in global carbon budgets. In support of our suggested upward revision, we note that the river carbon discharge has reported 2-sigma uncertainties of 100%^{53,54}. Only 60% of ocean-draining continental areas are monitored, and extreme events not captured by traditional monthly sampling (storms and floods) may contribute 50% to the annual carbon discharge^{55,56}. Furthermore, relatively low carbon discharge estimates³⁸ are tied to water budgets, which might underestimate drainage by ~50% compared to gauge measurements⁵⁵.

Additional uncertainties arise from the poorly-quantified carbon exchanges in inland and coastal waters⁵⁴ and with carbon-rich groundwaters^{57,58}. While the river flux uncertainty was always acknowledged to be large, we point out that there might be a systematic underestimation of its contribution in the context of global carbon budgets.

Uncertainties and caveats

We acknowledge that our revision of the river component is subject to considerable uncertainty. Errors in the pCO₂-based flux associated with wind, skin temperature effects^{47,59} and undersampling⁶⁰, could compensate for errors in the river flux. Considering an extreme scenario in which the contemporary air-sea flux is underestimated by 20% in the northern extra-tropics would add 0.1 PgC/y of southward transport, such that an upward revision of the river flux would no longer be needed to match the heat constraint. If the contemporary air-sea flux is also underestimated by 20% in the south, the upward revision would however still be required. Other sources of uncertainty are the Arctic air-sea flux and the human-induced increase in riverine carbon flux, both believed to be small enough that their uncertainties are not a major factor in this comparison (0.1±0.05 PgC/y each yields uncertainty in $A_C < 0.03$ PgC/y)^{53,61}. These possible trade-offs between ocean and river fluxes have however very little impact on the land flux estimate that depends on the sum of the ocean and river components.

Our study is based on a single atmospheric transport model, but our conclusions regarding the sensitivity of land fluxes to ocean priors cannot be strongly dependent on the model choice. Because inverse calculations effectively constrain the sum of land and ocean sinks within

latitude bands ^{2,21}, the sensitivity of the inferred land sinks to a shift in the ocean fluxes must be shared across atmospheric models.

In this study, we identified a systematic bias across a suite of ocean models that has a bearing on their use for assessing land sinks distribution. Dominant biases result from deficiencies in the physical transport and underscore the need for improvements in the representation of the meridional overturning circulation and its impact on heat and carbon transport. Large uncertainties in the biological pump limit the understanding of the global carbon cycle but are of second order. Within our model suite, those with the most realistic carbon asymmetries are models that combine a strong heat asymmetry and a strong iron-limitation of primary productivity in the Southern Ocean (see SI). We also show that it is possible to establish carbon fluxes matching observational heat transport constraints by combining contemporary pCO₂ observations and a natural river discharge of carbon larger than recent estimates. This calls for improvements in river carbon transport estimates and the more systematic treatment of rivers in carbon budgets. The river loop that carries carbon from land to ocean is usually implicitly allocated to either the ocean (ocean inversions) or land (atmospheric inversions). Yet, this loop is mostly a natural steady-state feature that should be separated from the transient sinks when discussing anthropogenic changes. This distinction becomes more important if the river fluxes are subject to upwards revision.

Materials and Methods

Observations of meridional transports of heat and pre-industrial carbon in Atlantic Ocean.

Estimates based on hydrographic data of ocean pre-industrial carbon meridional transport are only available for the Atlantic Ocean. Table S1 details the observations of heat and pre-industrial carbon used for Figure 1. Hydrographic data used for Figure 1 A were corrected for the influence of excess anthropogenic CO₂^{14,48}.

Definition of carbon transport asymmetry (A_C), heat asymmetry (A_Q) and biological pump asymmetry (A_{BioPump}).

The ocean transport asymmetry (A) is computed for carbon (A_C) and heat (A_Q) as the average of the steady-state northward transports across 20°N (T_N) and 20°S (T_S) (see Fig. 2):

$$A = (T_N + T_S) / 2 \quad \text{with } T \text{ and } A \text{ positive northward.}$$

In steady state, A must equal half of the difference between the net air-sea flux (plus the river discharge for A_C) north of 20°N (F_N) minus the flux south of 20°S (F_S).

$$A = (F_N - F_S) / 2 \quad \text{with } F \text{ positive into the atmosphere.}$$

This definition, which is not sensitive to air-sea fluxes in the tropics (20°S to 20°N), limits the impact of uncertainties on the tropical ocean and atmosphere dynamics, and provides a better metric of large-scale interhemispheric exchanges.

Carbon fluxes include air-sea fluxes and river discharge ($F_N = F_{N \text{ air-sea}} + F_{N \text{ river}}$, $F_S = F_{S \text{ air-sea}} + F_{S \text{ river}}$), while heat fluxes include air-sea fluxes only ($F_N = F_{N \text{ air-sea}}$, $F_S = F_{S \text{ air-sea}}$). As a result, A_C can be written as the sum of air-sea exchanges ($A_{\text{air-sea}}$) and river discharge (A_{riv}) contributions:

$$A_C = A_{\text{air-sea}} + A_{\text{riv}}$$

$$\text{where } A_{\text{air-sea}} = (F_{N \text{ air-sea}} - F_{S \text{ air-sea}})/2 \text{ and } A_{\text{river}} = (F_{N \text{ river}} - F_{S \text{ river}})/2$$

We define the biological pump asymmetry similarly to A_C , as the difference between the biogenic particulate carbon flux exported below 100 m south of 20°S (E_S , positive downward) minus the flux north of 20°N (E_N , positive downward) (Fig 2).

$$A_{\text{BioPump}} = (E_S - E_N) / 2$$

A_{BioPump} represents the imbalance between the carbon particulate export south of 20°S and north of 20°N, and hence the maximum amount of carbon of biological origin available for inter-hemispheric transport (not all of the available carbon is transported).

Earth-system and ocean models: transport, asymmetries and uncertainty.

We used the steady-state pre-industrial air-sea fluxes of CO₂ and heat from 9 Earth-system models (ESMs) and 2 ocean models (Tab. S2). Seven of the nine ESMs participated in the Coupled Model Intercomparison Project Phase 5 (CMIP5): the Community Earth System Model CESM version CESM1-BGC, two versions of the Geophysical Fluid Dynamics Laboratory (GFDL) Earth System Models (ESM2M with a nominally level vertical coordinate, and the ESM2G with a density-based layered vertical oceans)^{62,63}; the Institut Pierre-Simon Laplace Coupled Model 5, version IPSL-CM5A-LR⁶⁴; two versions of the Max Planck Institut für Meteorologie Earth System Model (low and medium resolution ocean: MPI-ESM-LR MPI-ESM-MR)⁶⁵; the Norwegian Earth System Model (NorESM1-ME)⁶⁶. We also added the pre-industrial control simulation of two recent large-ensemble experiments from the CESM model (CESM-LE)^{67,68} and the GFDL model (GFDL-LE). Finally, we used two versions of the NEMO-PISCES ocean model (NEMO 3.6 - PISCESv2): a standard version⁶⁹ and a sensitivity perturbation experiment for which the constraint of iron limitation is removed.

We only used quasi-equilibrated pre-industrial control simulations. For these simulations the drift in surface fluxes was small and corrected using linear regressions (drifts $< 5 \times 10^{-4}$ PgC/y and $< 10^{-5}$ PW in all models), and imbalances between ocean heat content and heat fluxes (< 0.03 PW) and between carbon inventory and carbon fluxes (< 0.02 PgC/y) were also small^{70,71}. We account for these imbalances in the uncertainties in A_C and A_Q . Model transports were computed from the multi-century mean pre-industrial air-sea fluxes to isolate the natural steady-state transport. Model sections on Figure 1 are at 30°S, 28°S, 23°S, 20°S, 15°S, 10°S, 5°S, 5°N, 10°N, 20°N, 30°N, 40°N, 50°N and 60°N.

The uncertainty on the asymmetry derived from the ESMs includes the interannual variability in the ocean transport (± 1 standard deviation over the simulation period) and the uncertainty associated with the imbalance in the carbon and heat budgets (0.02 PgC/y and 0.03 PW) for A_C and A_Q , and the uncertainty in the riverine discharge for A_C (see details on river below). We assume a 50% uncertainty on the northern and southern riverine carbon discharge, which leads to a 0.1 PgC/y uncertainty on A_C . The total uncertainty on A_C ranges from 0.17 to 0.23 PgC/y across the ESMs.

Asymmetries from existing ocean and river carbon flux estimates

The carbon transport asymmetry A_C was computed directly **from inversion-based pre-industrial ocean carbon fluxes**^{37,41} (Case A on Fig. 4). Unlike previous studies that removed an estimate of the river contribution from inversion results to focus more specifically on air-sea CO₂ fluxes^{38,41}, we retain the raw inversion results so that the river discharge is included in the computation of A_C . Uncertainties on Fig 4 **are as reported in the original study**³⁷ **and represent the spread across inverse models.**

A_C was computed for four different pCO₂-based estimates (Cases B-E on Fig. 4). In these four cases, A_C was computed by correcting pCO₂ contemporary air-sea fluxes⁴⁴⁻⁴⁶ with the anthropogenic carbon uptake estimate of Khatiwala and co-authors^{14,48} and by adding estimates of the river carbon discharge (see details on river correction below). Our best estimate of the ocean/river fluxes combines the pCO₂-based air-sea flux of Rödenbeck et al⁴⁴, corrected for anthropogenic carbon uptake^{14,48} and by correcting for a river flux of 0.78 PgC/y so that mass

conservation is ensured and better agreement with the heat-based constraint is reached. Note that any of the pCO₂-based product would give similar result (Fig. 4). Uncertainties on the pre-industrial air-sea flux reported in Tab S5 are computed as the standard error of the uncertainties in anthropogenic, riverine and pCO₂-based air-sea fluxes. Error bars on Fig. 4 are computed from the uncertainties reported in Tables S3, S4 and S5.

River carbon discharge correction

In Eq. (1), $A_C = A_{\text{air-sea}} + A_{\text{river}}$, where $A_{\text{air-sea}}$ is the air-sea flux contribution (excluding outgassing linked to river effects) and A_{river} is the river loop contribution to interhemispheric exchange (see Fig S6). We applied different levels of corrections for this river contribution to A_C .

All models include river freshwater inputs but not necessarily the associated carbon discharge. Three models (IPSL-CM5A-LR, NEMO-PISCES with and without iron limitation) include a riverine carbon discharge of 0.45 PgC/y in line with the estimate of Jacobson et al.³⁸, directly yielding A_C . GFDL-ESM2M and GFDL-ESM2G include part of the riverine carbon discharge (0.1 PgC/y) to compensate the steady-state calcite precipitation in sediments. All other ESMs do not include any river carbon discharge. As shown on Fig. S6, we add to all simulated values of A_C (except IPSL-CM5A-LR and the two NEMO-PISCES models) a southward contribution of -0.15 ± 0.05 PgC/y, which is consistent with the riverine discharge of Jacobson et al.³⁸ that contributes a riverine contribution of $A_{\text{riv}} = -0.10$ PgC/y and the associated pattern of CO₂ efflux of Aumont et al.¹⁷ that adds a southward transport of -0.05 PgC/y to A_{airsea} (outgassing compensating the river input at steady-state, see standard scenario on their Fig. 2b). Note that we ignore the small amount of carbon already accounted for in the two GFDL models. Although we

suggest in this study that the river estimate of 0.45 PgC/y needs upward revision (0.78 PgC/y), Eq. (1) would not be very sensitive to this revision, changing A_C by only -0.06 PgC/y and having no impact on the -0.31 and 0.19 regression factors.

pCO₂-based carbon fluxes include the CO₂ outgassing via air-sea flux associated with the river carbon discharge (F_{efflux} on Fig S6) but not the discharge itself⁴² (F_{river} on Fig S6). We used the pattern and magnitude of the river carbon discharge F_{river} of Jacobson et al³⁸ in cases B, C and D of Fig. 4 (0.45 PgC/y), and a scaled up version of that same pattern that matches a total inflow of 0.78 PgC/y in case E (Fig 4). Finally, ocean inverse calculations of carbon fluxes implicitly include rivers and do not require any correction⁴².

Land sink estimates based on two sets of ocean/river fluxes.

We computed the land sinks using the Jena CarboScope CO₂ inversion over the period 1990-2010, representing an update of Rödenbeck and coauthors⁴⁹. We performed two atmospheric inverse calculations, one **using ocean inversion-based ocean/river fluxes (Fig 5a) and one using pCO₂-based ocean/river fluxes (Fig 5b). In both atmospheric inversions, the ocean flux is prescribed as a fixed prior without adjustments (i.e. the ocean posterior flux equals the ocean prior flux). Case 1 uses the ocean inversion-based ocean/river fluxes reported by Gruber et al⁴¹ combined with the anthropogenic trend from 1990 to 2010 from Khatiwala and collaborators^{14,48} (Case A on Fig 4). Case 2 uses the monthly 1990-2010 climatological air-sea CO₂ flux based on ocean pCO₂ data⁴⁴ (updated version oc_v1.2) (Case E on Fig 4). In case 2, we also use the 1990 to 2010 anthropogenic trend from Khatiwala and**

collaborators^{14,48} to isolate the anthropogenic component from the natural component (see Fig 5 b).

A fundamental difference between the two inversions is the way the riverine input is accounted for. The prescribed ocean flux of case 1 includes both the air-sea and the river fluxes, whereas the prescribed ocean flux of case 2 only includes the air-sea CO₂ flux and exclude the river discharge. Rivers are therefore accounted for in the prescribed ocean sink in case 1 and in the land sink posterior in case 2. To compare both inversions, we separate the river discharge from the land sink in inversion case 2. Figure 5, Table S4 and Table S5 present the results for cases 1 and 2.

Acknowledgments: We thank four anonymous reviewers for their constructive and insightful comments. L. R. was granted support by the Climate Program Office of the National Oceanic and Atmospheric Administration grant NA13OAR4310219. S. K. was supported by US NSF grant OCE 10-60804. K. B. R. was supported by NASA award NNX14AL85G. NCAR is sponsored by the National Science Foundation. We also thank the groups developing MOM, MITgcm, NEMO and CMIP5 models for providing their model results.

Author contributions. L.R. directed the analysis of the several data sets used here and shared responsibility for writing the manuscript; R. F. K. and B. B. S. shared responsibility for writing the manuscript; C. R. computed the land sinks; L. B., M. C. L., K. B. R. provided model results. All authors contributed to the final version of the manuscript.

Additional information. Supplementary information is available in the online version of the

paper. Correspondence and requests for materials should be addressed to L.R.

Competing financial interests. The authors declare no competing financial interests.

Data Availability. Model data are available through the modeling centers and the CMIP5 database (cmip.llnl.gov/cmip5/data_portal.html). Scripps CO₂ data used in Figure 6 are available online at scrippsco2.ucsd.edu/data/atmospheric_co2. Results of the atmospheric inversion can be obtained upon request.

Code Availability. The code for the Jena Inversion model is available online at www.bgc-jena.mpg.de/~christian.roedenbeck/INVERSION/HOWTO/ or on request to the corresponding author.

References

1. Tans, P. P., Fung, I. Y. & Takahashi, T. Observational Constrains on the Global Atmospheric CO₂ Budget. *Science* **247**, 1431–1438 (1990).
2. Peylin, P. *et al.* Global atmospheric carbon budget: results from an ensemble of atmospheric CO₂ inversions. *Biogeosciences* **10**, 6699–6720 (2013).
3. Pan, Y. *et al.* A Large and Persistent Carbon Sink in the World's Forests. *Science* **333**, 988–993 (2011).
4. Sarmiento, J. L. *et al.* Trends and regional distributions of land and ocean carbon sinks. *Biogeosciences* **7**, 2351–2367 (2010).

- 445 5. Keeling, C. D., Piper, S. C., Whorf, T. P. & Keeling, R. F. Evolution of natural and
446 anthropogenic fluxes of atmospheric CO₂ from 1957 to 2003. *Tellus B* **63**, 1–22 (2011).
- 447 6. Schimel, D., Stephens, B. B. & Fisher, J. B. Effect of increasing CO₂ on the terrestrial carbon
448 cycle. *Proc. Natl. Acad. Sci.* **112**, 436–441 (2015).
- 449 7. Graven, H. D. *et al.* Enhanced Seasonal Exchange of CO₂ by Northern Ecosystems Since
450 1960. *Science* **341**, 1085–1089 (2013).
- 451 8. Forkel, M. *et al.* Enhanced seasonal CO₂ exchange caused by amplified plant productivity in
452 northern ecosystems. *Science* aac4971 (2016). doi:10.1126/science.aac4971
- 453 9. Quéré, C. L. *et al.* Global Carbon Budget 2016. *Earth Syst. Sci. Data* **8**, 605–649 (2016).
- 454 10. Bousquet, P. *et al.* Regional Changes in Carbon Dioxide Fluxes of Land and Oceans Since
455 1980. *Science* **290**, 1342–1346 (2000).
- 456 11. Stephens, B. B. *et al.* Weak Northern and Strong Tropical Land Carbon Uptake from
457 Vertical Profiles of Atmospheric CO₂. *Science* **316**, 1732–1735 (2007).
- 458 12. Andres, R. J. *et al.* A synthesis of carbon dioxide emissions from fossil-fuel combustion.
459 *Biogeosciences* **9**, 1845–1871 (2012).
- 460 13. Denning, A. S., Fung, I. Y. & Randall, D. Latitudinal gradient of atmospheric CO₂ due to
461 seasonal exchange with land biota. *Nature* **376**, 240–243 (1995).
- 462 14. Khatiwala, S., Primeau, F. & Hall, T. Reconstruction of the history of anthropogenic CO₂
463 concentrations in the ocean. *Nature* **462**, 346–349 (2009).
- 464 15. Broecker, W. S. & Peng, T.-H. Interhemispheric transport of carbon dioxide by ocean
465 circulation. *Nature* **356**, 587–589 (1992).
- 466 16. Sarmiento, J. L. & Sundquist, E. T. Revised budget for the oceanic uptake of anthropogenic
467 carbon dioxide. *Nature* **356**, 589–593 (1992).

- 468 17. Aumont, O. *et al.* Riverine-driven interhemispheric transport of carbon. *Glob. Biogeochem.*
469 *Cycles* **15**, 393–405 (2001).
- 470 18. Keeling, C. D., Piper, S. C. & Heimann, M. A three-dimensional model of atmospheric CO₂
471 transport based on observed winds: 4. Mean annual gradients and interannual variations. in
472 *Aspects of Climate Variability in the Pacific and the Western Americas* (ed. Peterson, D. H.)
473 305–363 (American Geophysical Union, 1989).
- 474 19. Gurney, K. R. *et al.* High Resolution Fossil Fuel Combustion CO₂ Emission Fluxes for the
475 United States. *Environ. Sci. Technol.* **43**, 5535–5541 (2009).
- 476 20. Olivier, J. G. J., Janssens-Maenhout, G., Muntean, M. & Peters, J. A. H. W. Trends in global
477 CO₂ emissions: 2016 Report - PBL Netherlands Environmental Assessment Agency. (2016).
478 Available at: <http://www.pbl.nl/en/publications/trends-in-global-co2-emissions-2016-report>.
479 (Accessed: 16th July 2017)
- 480 21. Steinkamp, K. & Gruber, N. A joint atmosphere-ocean inversion for the estimation of
481 seasonal carbon sources and sinks. *Glob. Biogeochem. Cycles* **27**, 732–745 (2013).
- 482 22. Houghton, R. A. Why are estimates of the terrestrial carbon balance so different? *Glob.*
483 *Change Biol.* **9**, 500–509 (2003).
- 484 23. Houghton, R. A. *et al.* Carbon emissions from land use and land-cover change.
485 *Biogeosciences* **9**, 5125–5142 (2012).
- 486 24. Brewer, P. G., Goyet, C. & Dyrssen, D. Carbon Dioxide Transport by Ocean Currents at
487 25°N Latitude in the Atlantic Ocean. *Science* **246**, 477–479 (1989).
- 488 25. Keeling, R. F. & Peng, T.-H. Transport of Heat, CO₂ and O₂ by the Atlantic's Thermohaline
489 Circulation. *Philos. Trans. R. Soc. Lond. B Biol. Sci.* **348**, 133–142 (1995).

- 490 26. Large, W. G. & Yeager, S. G. The global climatology of an interannually varying air–sea
491 flux data set. *Clim. Dyn.* **33**, 341–364 (2009).
- 492 27. Resplandy, L. *et al.* Constraints on oceanic meridional heat transport from combined
493 measurements of oxygen and carbon. *Clim. Dyn.* **47**, 3335 (2016).
- 494 28. Ganachaud, A. & Wunsch, C. Large-Scale Ocean Heat and Freshwater Transports during the
495 World Ocean Circulation Experiment. *J. Clim.* **16**, 696–705 (2003).
- 496 29. Schlitzer, R. Applying the Adjoint Method for Biogeochemical Modeling: Export of
497 Particulate Organic Matter in the World Ocean. in *Inverse Methods in Global*
498 *Biogeochemical Cycles* (eds. Kasibhatla, P. *et al.*) 107–124 (American Geophysical Union,
499 2000). doi:10.1029/GM114p0107
- 500 30. Henson, S. A. *et al.* Rapid emergence of climate change in environmental drivers of marine
501 ecosystems. *Nat. Commun.* **8**, 14682 (2017).
- 502 31. Siegel, D. A. *et al.* Global assessment of ocean carbon export by combining satellite
503 observations and food-web models. *Glob. Biogeochem. Cycles* **28**, 181–196 (2014).
- 504 32. DeVries, T. & Weber, T. The export and fate of organic matter in the ocean: New constraints
505 from combining satellite and oceanographic tracer observations. *Glob. Biogeochem. Cycles*
506 **31**, 2016GB005551 (2017).
- 507 33. Yeager, S. & Danabasoglu, G. Sensitivity of Atlantic Meridional Overturning Circulation
508 Variability to Parameterized Nordic Sea Overflows in CCSM4. *J. Clim.* **25**, 2077–2103
509 (2011).
- 510 34. Wang, C., Zhang, L., Lee, S.-K., Wu, L. & Mechoso, C. R. A global perspective on CMIP5
511 climate model biases. *Nat. Clim. Change* **4**, 201–205 (2014).

- 512 35. Ma, X. *et al.* Western boundary currents regulated by interaction between ocean eddies and
513 the atmosphere. *Nature* **535**, 533–537 (2016).
- 514 36. Doney, S. C. *et al.* Evaluating global ocean carbon models: The importance of realistic
515 physics. *Glob. Biogeochem. Cycles* **18**, GB3017 (2004).
- 516 37. Mikaloff Fletcher, S. E. *et al.* Inverse estimates of the oceanic sources and sinks of natural
517 CO₂ and the implied oceanic carbon transport. *Glob. Biogeochem. Cycles* **21**, GB1010
518 (2007).
- 519 38. Jacobson, A. R., Mikaloff Fletcher, S. E., Gruber, N., Sarmiento, J. L. & Gloor, M. A joint
520 atmosphere-ocean inversion for surface fluxes of carbon dioxide: 1. Methods and global-
521 scale fluxes. *Glob. Biogeochem. Cycles* **21**, GB1019 (2007).
- 522 39. Gerber, M. & Joos, F. Carbon sources and sinks from an Ensemble Kalman Filter ocean data
523 assimilation. *Glob. Biogeochem. Cycles* **24**, GB3004 (2010).
- 524 40. DeVries, T. The oceanic anthropogenic CO₂ sink: Storage, air-sea fluxes, and transports over
525 the industrial era. *Glob. Biogeochem. Cycles* **28**, 631–647 (2014).
- 526 41. Gruber, N. *et al.* Oceanic sources, sinks, and transport of atmospheric CO₂. *Glob.*
527 *Biogeochem. Cycles* **23**, GB1005 (2009).
- 528 42. Sarmiento, J. L. *et al.* Sea-air CO₂ fluxes and carbon transport: A comparison of three ocean
529 general circulation models. *Glob. Biogeochem. Cycles* **14**, 1267–1281 (2000).
- 530 43. Murnane, R. J., Sarmiento, J. L. & Le Quéré, C. Spatial distribution of air-sea CO₂ fluxes
531 and the interhemispheric transport of carbon by the oceans. *Glob. Biogeochem. Cycles* **13**,
532 287–305 (1999).
- 533 44. Rödenbeck, C. *et al.* Global surface-ocean pCO₂ and sea–air CO₂ flux variability from an
534 observation-driven ocean mixed-layer scheme. *Ocean Sci.* **9**, 193–216 (2013).

- 535 45. Takahashi, T. *et al.* Climatological mean and decadal change in surface ocean pCO₂, and net
536 sea–air CO₂ flux over the global oceans. *Deep Sea Res. Part II Top. Stud. Oceanogr.* **56**,
537 554–577 (2009).
- 538 46. Landschützer, P., Gruber, N., Bakker, D. C. E. & Schuster, U. Recent variability of the
539 global ocean carbon sink. *Glob. Biogeochem. Cycles* **28**, 927–949 (2014).
- 540 47. Wanninkhof, R. *et al.* Global ocean carbon uptake: magnitude, variability and trends.
541 *Biogeosciences* **10**, 1983–2000 (2013).
- 542 48. Khatiwala, S. *et al.* Global ocean storage of anthropogenic carbon. *Biogeosciences* **10**, 2169–
543 2191 (2013).
- 544 49. Rödenbeck, C., Houweling, S., Gloor, M. & Heimann, M. CO₂ flux history 1982–2001
545 inferred from atmospheric data using a global inversion of atmospheric transport. *Atmos*
546 *Chem Phys* **3**, 1919–1964 (2003).
- 547 50. Grace, J., Mitchard, E. & Gloor, E. Perturbations in the carbon budget of the tropics. *Glob.*
548 *Change Biol.* **20**, 3238–3255 (2014).
- 549 51. Conway, T. J. & Tans, P. P. Development of the CO₂ latitude gradient in recent decades.
550 *Glob. Biogeochem. Cycles* **13**, 821–826 (1999).
- 551 52. Fan, S. *et al.* A Large Terrestrial Carbon Sink in North America Implied by Atmospheric and
552 Oceanic Carbon Dioxide Data and Models. *Science* **282**, 442–446 (1998).
- 553 53. Regnier, P. *et al.* Anthropogenic perturbation of the carbon fluxes from land to ocean. *Nat.*
554 *Geosci.* **6**, 597–607 (2013).
- 555 54. Bauer, J. E. *et al.* The changing carbon cycle of the coastal ocean. *Nature* **504**, 61–70 (2013).
- 556 55. Clark, E. A., Sheffield, J., van Vliet, M. T. H., Nijssen, B. & Lettenmaier, D. P. Continental
557 Runoff into the Oceans (1950–2008). *J. Hydrometeorol.* **16**, 1502–1520 (2015).

56. Bianchi, T. S. *et al.* Enhanced transfer of terrestrially derived carbon to the atmosphere in a flooding event. *Geophys. Res. Lett.* **40**, 116–122 (2013).
57. Kwon, E. Y. *et al.* Global estimate of submarine groundwater discharge based on an observationally constrained radium isotope model. *Geophys. Res. Lett.* **41**, 8438–8444 (2014).
58. Le Gland, G., Mémery, L., Aumont, O. & Resplandy, L. Improving the inverse modeling of a trace isotope: how precisely can radium-228 fluxes toward the ocean and submarine groundwater discharge be estimated? *Biogeosciences* **14**, 3171–3189 (2017).
59. Woolf, D. K., Land, P. E., Shutler, J. D., Goddijn-Murphy, L. M. & Donlon, C. J. On the calculation of air-sea fluxes of CO₂ in the presence of temperature and salinity gradients: AIR-SEA CO₂ FLUXES. *J. Geophys. Res. Oceans* **121**, 1229–1248 (2016).
60. Rödenbeck, C. *et al.* Data-based estimates of the ocean carbon sink variability – first results of the Surface Ocean pCO₂ Mapping intercomparison (SOCOM). *Biogeosciences* **12**, 7251–7278 (2015).
61. Schuster, U. *et al.* An assessment of the Atlantic and Arctic sea–air CO₂ fluxes, 1990–2009. *Biogeosciences* **10**, 607–627 (2013).
62. Dunne, J. P. *et al.* GFDL’s ESM2 Global Coupled Climate–Carbon Earth System Models. Part I: Physical Formulation and Baseline Simulation Characteristics. *J. Clim.* **25**, 6646–6665 (2012).
63. Dunne, J. P. *et al.* GFDL’s ESM2 Global Coupled Climate–Carbon Earth System Models. Part II: Carbon System Formulation and Baseline Simulation Characteristics. *J. Clim.* **26**, 2247–2267 (2013).

- 580 64. Séférian, R., Iudicone, D., Bopp, L., Roy, T. & Madec, G. Water Mass Analysis of Effect of
581 Climate Change on Air–Sea CO₂ Fluxes: The Southern Ocean. *J. Clim.* **25**, 3894–3908
582 (2012).
- 583 65. Ilyina, T. *et al.* Global ocean biogeochemistry model HAMOCC: Model architecture and
584 performance as component of the MPI-Earth system model in different CMIP5 experimental
585 realizations. *J. Adv. Model. Earth Syst.* **5**, 287–315 (2013).
- 586 66. Tjiputra, J. F. *et al.* Evaluation of the carbon cycle components in the Norwegian Earth
587 System Model (NorESM). *Geosci Model Dev* **6**, 301–325 (2013).
- 588 67. Long, M. C., Deutsch, C. & Ito, T. Finding forced trends in oceanic oxygen. *Glob.*
589 *Biogeochem. Cycles* **30**, 2015GB005310 (2016).
- 590 68. Kay, J. E. *et al.* The Community Earth System Model (CESM) Large Ensemble Project: A
591 Community Resource for Studying Climate Change in the Presence of Internal Climate
592 Variability. *Bull. Am. Meteorol. Soc.* **96**, 1333–1349 (2014).
- 593 69. Aumont, O., Ethé, C., Tagliabue, A., Bopp, L. & Gehlen, M. PISCES-v2: an ocean
594 biogeochemical model for carbon and ecosystem studies. *Geosci. Model Dev.* **8**, 2465–2513
595 (2015).
- 596 70. Hobbs, W., Palmer, M. D. & Monselesan, D. An Energy Conservation Analysis of Ocean
597 Drift in the CMIP5 Global Coupled Models. *J. Clim.* **29**, 1639–1653 (2015).
- 598 71. Séférian, R. *et al.* Inconsistent strategies to spin up models in CMIP5: implications for ocean
599 biogeochemical model performance assessment. *Geosci. Model Dev.* **9**, 1827–1851 (2016).
- 600 72. Lundberg, L. & Haugan, P. M. A Nordic Seas–Arctic Ocean carbon budget from volume
601 flows and inorganic carbon data. *Glob. Biogeochem. Cycles* **10**, 493–510 (1996).

- 602 73. Macdonald, A. M., Baringer, M. O., Wanninkhof, R., Lee, K. & Wallace, D. W. R. A 1998–
603 1992 comparison of inorganic carbon and its transport across 24.5°N in the Atlantic. *Deep*
604 *Sea Res. Part II Top. Stud. Oceanogr.* **50**, 3041–3064 (2003).
- 605 74. Holfort, J., Johnson, K. M., Schneider, B., Siedler, G. & Wallace, D. W. R. Meridional
606 transport of dissolved inorganic carbon in the South Atlantic Ocean. *Glob. Biogeochem.*
607 *Cycles* **12**, 479–499 (1998).
- 608 75. Álvarez, M., Ríos, A. F., Pérez, F. F., Bryden, H. L. & Rosón, G. Transports and budgets of
609 total inorganic carbon in the subpolar and temperate North Atlantic. *Glob. Biogeochem.*
610 *Cycles* **17**, 1002 (2003).
- 611 76. Johns, W. E. *et al.* Continuous, Array-Based Estimates of Atlantic Ocean Heat Transport at
612 26.5°N. *J. Clim.* **24**, 2429–2449 (2011).
- 613
- 614 Correspondence should be addressed to Laure Resplandy (laurer@princeton.edu)

Fig. 1. Overturning circulation and biological pump link carbon and heat transport in ocean basins. a) Meridional transports (positive northward) of preindustrial carbon and heat from hydrographic data in the Atlantic Ocean^{28,72-76} and from 11 models in the Atlantic and Indo-Pacific basins (no data in Indo-Pacific). Solid line is a fit to Atlantic Ocean data ($Y = -0.30 \times X - 0.15$). Models with weak (solid) and strong (dashed) biological-heat decoupling are circled; b) Overturning circulation pathways (solid), biologically-driven bi-directional exchanges of carbon at high latitudes (dashed), and c) their qualitative impact on the transport across 20°N and 20°S. AMOC: Atlantic meridional overturning circulation. Details in methods, Tab. S1 and S2.

Fig. 2. Schematic of ocean transport asymmetries. Transport asymmetries in a) carbon (A_C), b) heat (A_Q) and c) biological pump ($A_{BioPump}$). A_C and A_Q are the mean of steady-state ocean transports across 20°N and 20°S (T_S and T_N) and balance the northern and southern extratropical fluxes (F_N and F_S). $A_{BioPump}$ is the imbalance between the carbon particulate export below 100 m south of 20°S and north of 20°N (E_S and E_N). Transports (T) and asymmetries (A) are positive northward, air-sea fluxes (F) are positive towards the atmosphere and exports (E) are positive downwards.

Fig. 3. Link between heat and carbon asymmetries. Carbon asymmetry (A_C) as a function of heat asymmetry (A_Q) in 11 models and observational constraint on A_Q based on two independent estimates^{26 27} (grey shading). A_C is normalized using $A_{BioPump} = 2.2 \pm 0.1$ Pg C/yr (model ensemble mean ± 2 -sigma). Linear heat-to-carbon ratio (solid) and 2-sigma level confidence interval (dashed) are shown. Earth system and ocean models are CESM1-BGC (1), GFDL-

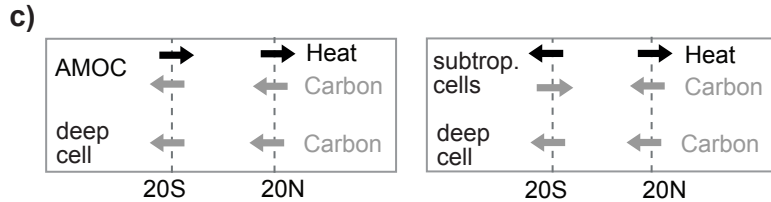
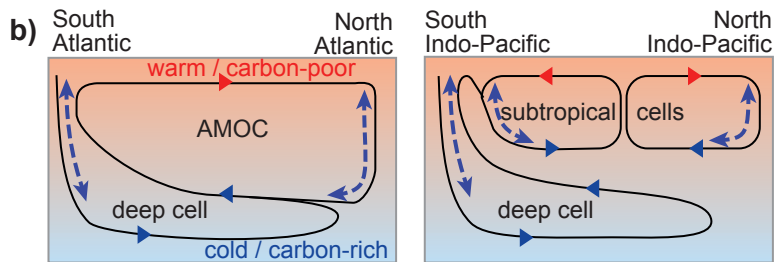
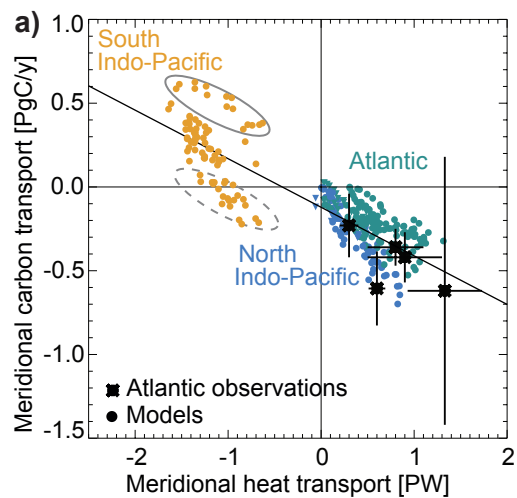
ESM2G (2), GFDL-ESM2M (3), IPSL-CM5A-LR (4), MPI-ESM-LR (5), MPI-ESM-MR (6),
NorESM1-ME (7), NEMO-PISCES with (8) and without (9) iron limitation, CESM-LE (10) and
GFDL-LE (11).

Fig. 4. Observation-based estimates of the carbon transport asymmetry A_C . A_C from ocean
inversions (A) and pCO₂-based estimates (B-E) is compared to the heat-based observational
constraint on $A_C = -0.52 \pm 0.15$ PgC/y (grey shading). Ocean inversion-based A_C derived from
preindustrial fluxes implicitly incorporate the impact of rivers^{37,41} (Tab S4). pCO₂-based
estimates for cases B⁴⁵, C⁴⁶ and D⁴⁴ are corrected for the anthropogenic uptake^{14,48} and the
river carbon discharge³⁸ (Tab. S3 and methods). pCO₂-based case E is case D with a scaled-up
river flux³⁸ of 0.78 PgC/y (Tab S5). Cases A and E are used to compute land sinks on Fig 5.

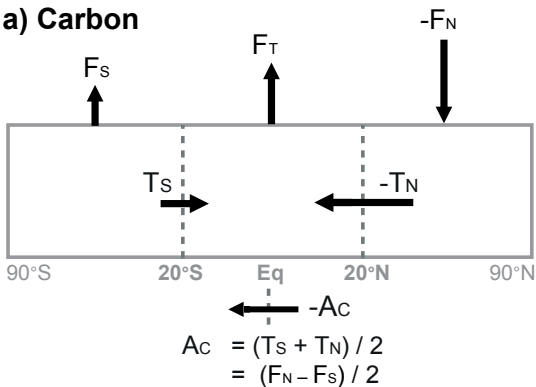
Fig. 5. Impact of ocean/river carbon asymmetry on land sinks. Land sinks obtained from the
Jena CarboScope CO₂ atmospheric inversion (1990-2010 average): a) with the ocean inversion-
based carbon fluxes (case A on Fig 4); and b) with pCO₂-based air-sea flux corrected for
anthropogenic carbon uptake and a scaled-up river flux of 0.78 PgC/y (case E on Fig 4). Pre-
industrial fluxes are in black, anthropogenic perturbations centered on year 2000 (1990-2010
average) are in red. Steady-state meridional transports of pre-industrial carbon across 20°S and
20°N are indicated in italic.

Fig. 6. Revised ocean/river flux is consistent with atmospheric CO₂ data. Observed Mauna
Loa (19.5°N, 155.6°W) to South Pole (90°S) gradient in atmospheric CO₂ between 1959 and

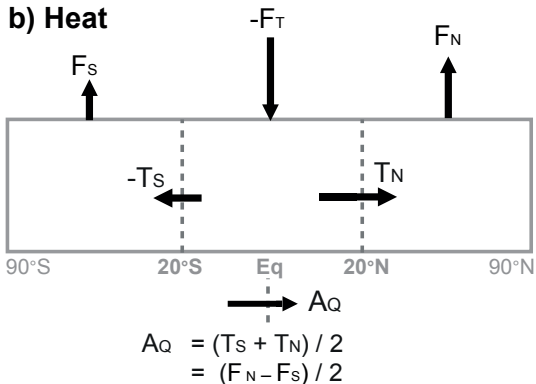
2014⁵ as a function of fossil fuel emissions⁹. Keeling and co-authors¹⁸ used the extrapolation back to zero emissions (y-intercept) to estimate the north-south pre-industrial gradient in atmospheric CO₂ assuming steady-state in land and ocean pre-industrial components. Following this method, the y-intercept gives a northern deficit of -0.55 ± 0.15 ppm, which is compatible with the Mauna Loa to South Pole gradient (grey shading) obtained by transporting our revised ocean/river flux with the TM3 atmospheric transport model (SI and Fig. S5).



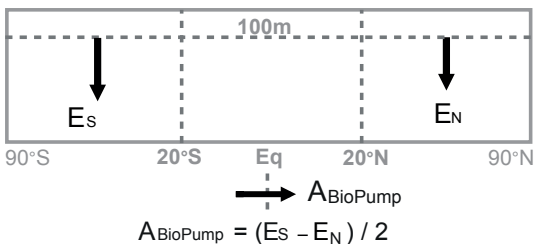
a) Carbon

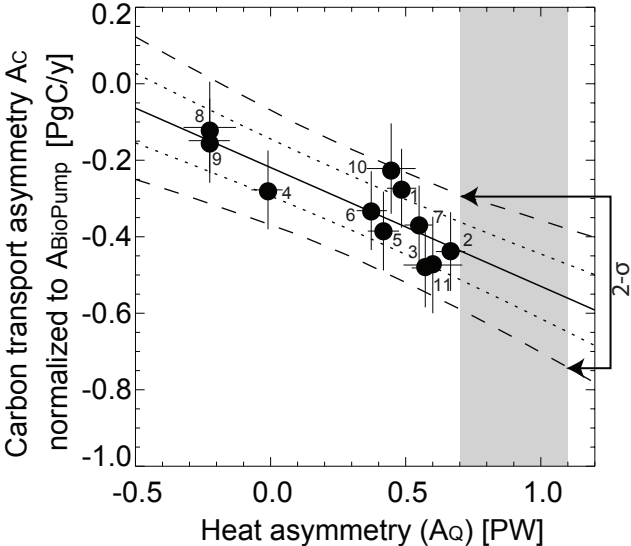


b) Heat



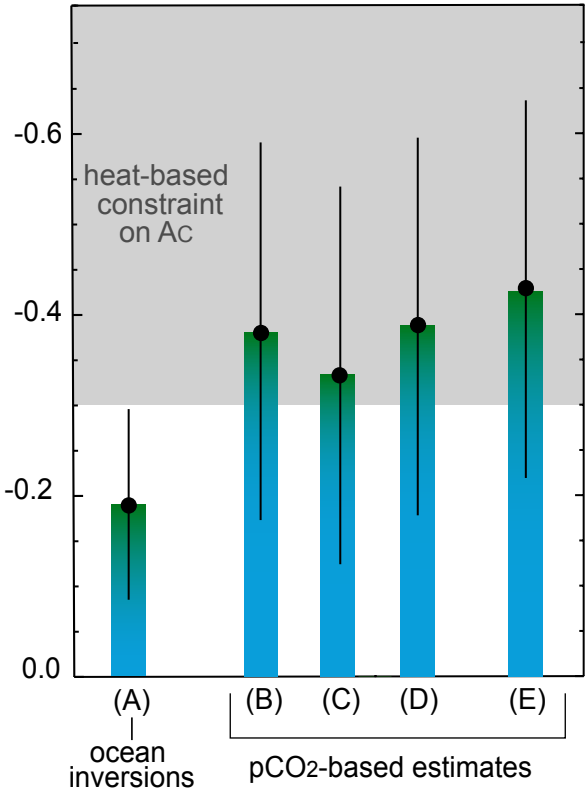
c) Biological pump



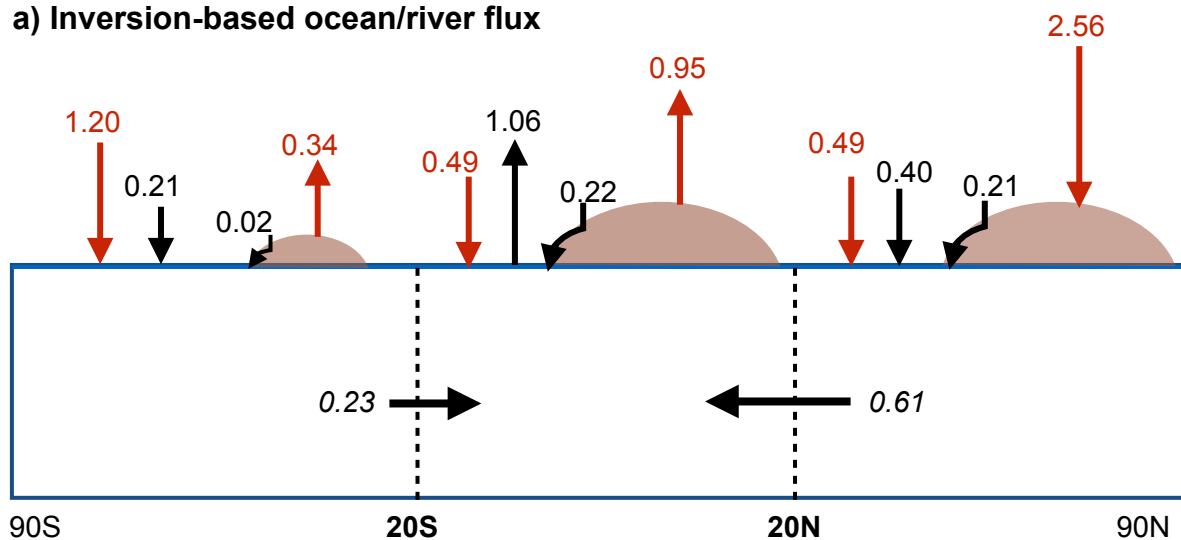


Carbon transport asymmetry

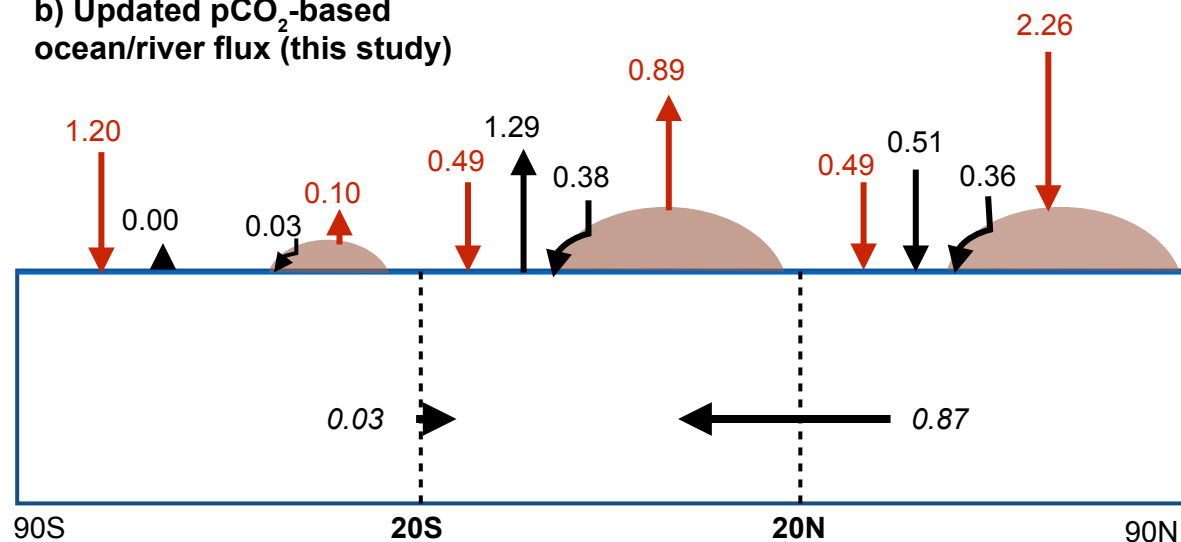
$$Ac = A_{\text{air-sea}} + A_{\text{riv}} \text{ [PgC/y]}$$



a) Inversion-based ocean/river flux



b) Updated pCO₂-based ocean/river flux (this study)



observed CO₂ gradient
Mauna Loa to South Pole [ppm]

